Ba Deposition and Oxidation on θ-Al_2O_3/NiAl(100) Ultrathin Films. Part I: Anaerobic Deposition Conditions

Emrah Ozensoy, Charles H. F. Peden, and János Szanyi*

Institute for Interfacial Catalysis, Pacific Northwest National Laboratory, P.O. Box 999, MSIN K8-93, Richland, Washington 99352

Received: January 31, 2006; In Final Form: May 19, 2006

Room-temperature Ba deposition on an oxygen-terminated θ-Al_2O_3/NiAl(100) ultrathin film substrate under ultrahigh vacuum (UHV) conditions is studied using X-ray photoelectron spectroscopy (XPS), Auger electron spectroscopy (AES) and temperature programmed desorption (TPD) techniques. In addition, Ba oxidation by the ions of the alumina substrate at 300 K < T < 1200 K in the absence of a gas-phase oxidizing agent is investigated. Our results indicate that at room temperature Ba grows in a layer-by-layer fashion for the first two layers, and Ba is partially oxidized. Annealing at T < 700 K results in further oxidation of the Ba species, whereas annealing at higher temperatures leads to loss of Ba from the surface via desorption and subsurface diffusion.

1. Introduction

Alkali earth metals have a wide variety of applications in chemical and materials technologies.[1−45] Recently, Ba compounds have attracted significant attention, due to the highly electropositive nature of Ba, leading to strongly ionic compounds where Ba cations induce strong fields that can result in materials with unique properties. Some important examples, where these interesting properties of Ba are utilized, can be found in high-T_c superconductor literature where Y−Ba−Cu−O (YBCO) based materials are intensely studied.[1−2] In addition, $BaTiO_3$ is used in semiconductor technology as a dielectric material in transistor architecture, and Ba metal is used in vacuum tubes as getters. Like most of the alkaline-earth metals, Ba dramatically decreases the work function of semiconductor surfaces.[3] Hence, Ba doping can also be used in electron emission sources.[4] Another application of Ba doping in semiconductor processes is related to the Ba/Si(111) and Ba/Si(100) interfaces where Ba metal is used to activate low-temperature silicon oxidation to form SiO_2.[3−10] It was suggested in a previous report that Ba deposition on Si surfaces can enhance low-temperature Si oxidation up to a factor of 5.[10]

These remarkable electronic properties of Ba-containing materials are apparent during Ba deposition and oxidation on surfaces where interesting Ba core-level shifts (varying from +0.5 eV to −1.6 eV) have been observed in previous XPS studies.[8−20] For many transition metals, binding energies shift to higher values upon oxidation. This is generally explained as a result of a screening charge withdrawal (leading to a decreased screening for the core levels) and changes in the final state screening.[14] Change in the final state screening is accomplished by the rearrangement of the conduction band electrons in metals, while in metal oxides, it is achieved by polarizing neighboring ions.[14] On the other hand, additional final state relaxation effects, in the form of charge transfer[46] from the O 2p to the cation shell, are also known to operate in oxides. The magnitude of the binding energy shifts (ΔBE) for the compounds of group IIa elements monotonically decreases going from Mg to Ba, where the relatively larger and positive ΔBE observed[24] for Mg becomes gradually smaller for Ca and Sr compounds and switches sign for Ba compounds, resulting in a negative ΔBE. Observation of a negative ΔBE upon oxidation is not exclusive to Ba compounds, as similar negative core level shifts have also been reported for Cu, Zn, Ag, Cd, and Cs compounds.[21−22]

A number of experimental as well as theoretical studies have discussed the origin of the negative binding energy shifts of oxidized Ba compounds with respect to that of the metallic Ba states:[11−18] (a) Wertheim[13] suggested that the experimentally observed negative ΔBE can be attributed to an increased population of the 5d states in BaO, with a $6s^{2-x}$ $5d^x$ valence state configuration, as opposed to metallic Ba having a $6s^2$ $5d^0$ configuration. This reasoning was based on charge flow from the delocalized conduction band to the spatially compact or localized 5d bonding states during oxide formation, which can ultimately provide an increase in the efficiency of the screening and thus lower the BE. (b) However, photoemission studies of Jacobi et al.[14] showed that, in sharp contrast to Wertheim's arguments, there exist some occupied 5d states in metallic Ba (i.e., $6s^{2-x}$ $5d^x$ valence state configuration), while BaO had a valence state configuration of $O2p^6$ Ba $6s^0 5d^0$, lacking any occupied 5d states. In this case, the authors proposed that a highly polarizable O^{2-} state in the BaO structure caused an enhanced final state screening and a negative ΔBE. (c) Hill et al.[16] argued against the presence of a highly polarizable O^{2-} state in BaO and further suggested that changes in the position of the Fermi level of the oxide was responsible for the observed negative ΔBE. This report also mentioned that such shifts were sensitive to the disorder/defects in the oxide material. (d) A different explanation was employed in a work by Vasquez,[17] where it was argued that lattice potential effects (i.e., existence of a Madelung potential, V_{Mad}, in the oxide lattice) and changes in the work function of the surface upon oxidation of the metallic surface can be used to account for the experimental observations. (e) Finally, Bagus and Pacchioni et al.[47,48] suggested that the BE trends observed for the oxidation of alkali earth metals originate from two different initial state electronic effects with opposite influences on the BE values. In other words, the change

* Corresponding author. E-mail: janos.szanyi@pnl.gov.

10.1021/jp060668l CCC: $33.50
Published on Web 08/08/2006

in the electrostatic potential due to the loss of ns orbitals upon oxidation (i.e., $M^0 \rightarrow M^{2+}$) tends to increase the BE values, whereas the Madelung potential arising from the existence of an ionic crystal tends to decrease the BE. values. Furthermore, these authors also reported that additional final state effects such as the polarization of the oxygen anion as a response to the core hole in the final ionized state or covalent bonding between metal and oxygen do not have a major influence in the observed trends. It should be noted that a sole consideration of V_{Mad} values is not sufficient to explain cation BE trends in group IIa metal oxides. For example, although the influence of V_{Mad} on the BE values is greater (in other words more negative) in MgO compared to BaO, as a consequence of a higher ionicity in MgO,[17,18,23] Mg oxidation results in a positive ΔBE.[24]

Ba compounds are also extensively used as promoters and performance enhancers in heterogeneous catalytic applications for a number of chemical processes. Among these, the NO_x storage reduction (NSR) technology,[25−28] where Pt/BaO/γ-Al_2O_3-based systems are used to reduce environmentally hazardous NO_x species originating from diesel engine emissions, has become an important alternative to the traditional selective catalytic reduction (SCR) approach. It should be noted that, due to the highly oxidizing environment resulting from the diesel engine operation, conventional Pt/Rh/γ-Al_2O_3 or Pd/γ-Al_2O_3-based three-way catalysts (TWC)[28−30] severely fail to reduce NO_x species. In contrast to the well-established understanding of the TWC systems, where some of the first published studies appeared as early as the beginning of 1970s, NSR technology was developed very recently, in 1994, by Toyota Motor Co.;[28] thus, a detailed molecular level understanding of these systems is not yet available. In the past decade, a majority of the scientific literature on the NSR systems has focused on high surface area Pt/BaO/γ-Al_2O_3- or BaO/γ-Al_2O_3-based supported catalysts.[25] There exist few surface science studies[31] investigating the fundamental chemical and surface phenomena that are relevant to the NSR technology.

Therefore, we have recently focused on using θ-Al_2O_3 ultrathin films grown on a NiAl(100) single-crystal bimetallic substrate as a model catalyst support to study NSR-related surface chemistry. Spectroscopic characterization of the θ-Al_2O_3/NiAl(100) model catalyst surface[32] and its interaction with H_2O,[32] NO_2,[33] and H_2O+NO_2[34] were previously investigated comprehensively in order to obtain insights regarding the behavior of the alumina support in the absence of the active Ba-containing phase. Here in this two-part series, we focus on the synthesis of the BaO/θ-Al_2O_3/NiAl(100) model NO_x storage material and investigate the Ba deposition and oxidation on θ-Al_2O_3 ultrathin films using various oxidation protocols. In the first part of this series (i.e., in the current text), room-temperature Ba deposition on an oxygen terminated θ-Al_2O_3/NiAl(100) ultrathin film substrate under ultrahigh vacuum (UHV) conditions is studied. In addition, Ba oxidation at $T > 300$ K in the absence of a gas-phase oxidizing agent is investigated using TPD, AES, and XPS techniques. In the second part of the series,[35] oxidation of Ba metal deposited on a θ-Al_2O_3/NiAl(100) ultrathin film with O_2(g) at various temperatures will be discussed in detail.

2. Experimental Section

Experiments reported in this work were performed in an ultrahigh vacuum (UHV) surface analysis chamber ($P_{base} = 2 \times 10^{-10}$ Torr) equipped with XPS, AES, a quadruple mass spectrometer (QMS) for TPD, and a rear-view low energy electron diffraction (LEED) setup. The NiAl(100) single crystal used in the experiments (Princeton Scientific Corp., 10 mm diameter, 2 mm thick) was polished on both sides and spot-welded onto a U-shaped Ta wire. A C-type thermocouple was spot welded to the top edge of the crystal for temperature measurements. The NiAl(100) crystal was cleaned by alternating cycles of Ar^+ ion sputtering ($V_{beam} = 1.5$ kV, $I_{beam} = 1.5\mu$A) and high-temperature UHV anneals at 1200 K. Cleanliness of the NiAl(100) sample was checked with AES and LEED.

Ultrathin θ-Al_2O_3 films on clean NiAl(100) were grown using a procedure that was originally developed by Ibach and co-workers[36,37] which included saturation of the NiAl(100) surface with O_2 at 300 K (total O_2 exposure = 9000 L; 1 L = 1×10^{-6} Torr s^{-1}), and successive annealing of the O-saturated surface at 1200 K in UHV (c.a. 60 min) in order to improve the crystallanity of the oxide film.[38−40] The quality of the θ-Al_2O_3 films was checked with AES, XPS, and LEED.[32] The typical initial thickness of these clean films prior to Ba deposition was 6 Å ± 2 Å.[32]

Ba deposition was performed via evaporation of Ba in UHV from an exothermic Ba ring getter (SAES Getters Inc.) doser. This doser was constructed by spot welding a short strip (~15 mm) of Ba getter material[41] to two Ta rods for resistive heating. The major components of the exothermic Ba ring getter material were powdered barium−aluminum alloy mixed with powdered nickel. Upon resistive heating of the getter material, a solid-state exothermic reaction starts to occur which results in a further rapid increase in the doser temperature. Elemental Ba evaporation takes place due to this exothermic reaction between the Al and Ni components of the getter material:

$$BaAl_4(s) + 4Ni(s) \rightarrow Ba(g) + 4NiAl(s) \qquad (1)$$

Before the experiments, the Ba doser was outgassed in UHV for an extended period of time to minimize contaminations. After having outgassed the doser, cleanliness of the deposits from the Ba doser was tested by performing Ba deposition on a clean metallic NiAl(100) surface. AES and XPS experiments showed no C-, O-, or N-containing species immediately after the Ba deposition. However, XPS and AES experiments performed after having kept the sample in UHV for > 40 min after the Ba deposition revealed that, due to its highly reactive nature, freshly deposited metallic Ba interacted with background gases such as H_2O (with partial pressures $< 1 \times 10^{-10}$ Torr) to form small but detectable amounts of O-containing species. For all of the Ba deposition experiments given here, the temperature of the θ-Al_2O_3/NiAl(100) surface was kept at 300 K during Ba evaporation.

TPD experiments were carried out using a differentially pumped QMS (UTI) by applying −70 V bias voltage on the spectrometer shield to constrain the ionizing electrons to the interior of the QMS shield, in order to prevent any possible electron beam damage on the sample. All of the TPD data presented in this study were obtained by ramping the temperature of the crystal at a constant rate of 2 K/s. Prior to each TPD experiment, the atomic mass unit (amu) scale of the QMS was calibrated for high amu values using Xe^{132}(g) which has a similar atomic weight to that of Ba^{138}, the most naturally abundant Ba isotope.

XPS data were acquired with a multichannel electrostatic hemispherical electron energy analyzer (Omicron, EA-125), using an MgKα X-ray source ($h\nu = 1253.6$ eV) and a 50 eV pass energy. The X-ray source was oriented ~50° with respect to the sample normal. Utilization of a bimetallic substrate and an ultrathin film oxide prevented the charging of the sample during the XPS experiments, which is evident by the binding

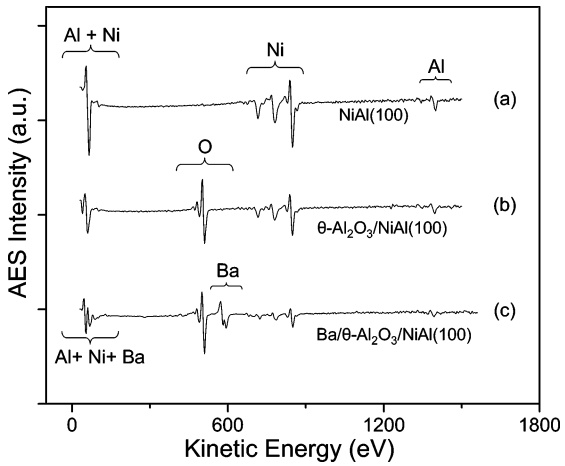

Figure 1. AES data for a clean NiAl(100) surface (a), a clean and oxygen terminated θ-Al_2O_3/NiAl(100) surface (b), and a θ-Al_2O_3/NiAl-(100) surface after ~1 ML Ba deposition at 300 K (c).

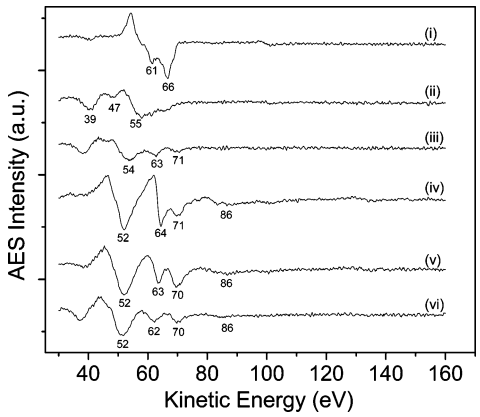

Figure 2. High-resolution AES data for selected deposition/preparation steps: (i) clean NiAl(100) surface; (ii) clean θ-Al_2O_3/NiAl(100) surface; (iii) 5 min Ba deposition ($\theta_{Ba} \ll 1$ ML) on θ-Al_2O_3/NiAl(100) surface at 300 K; (iv) 75 min Ba deposition ($\theta_{Ba} \sim 2$ML) on θ-Al_2O_3/NiAl-(100) surface at 300 K; (v) 75 min Ba deposition ($\theta_{Ba} \sim 2$ML) on θ-Al_2O_3/NiAl(100) at 300 K and subsequent annealing at 800 K in UHV; (vi) 75 min Ba deposition ($\theta_{Ba} \sim 2$ML) on θ-Al_2O_3/NiAl(100) at 300 K and subsequent annealing at 1200 K in UHV.

energy value of the Al $2p^0$ signal of the NiAl(100) substrate observed at 72.6 eV. A single-pass cylindrical mirror analyzer (CMA, PHI) was employed in the AES experiments with a primary beam energy of 3 kV. Sample positioning and other experimental parameters such as the elastic peak energy at a given sample position, multiplier voltages, and emission current values were routinely reproduced for each AES measurement.

3. Results and Discussion

3.1. Ba Deposition Procedures. Ba metal was first evaporated on a clean and oxygen-terminated θ-Al_2O_3/NiAl(100) surface at 300 K under UHV conditions in a step-by-step fashion (total number of Ba deposition steps = 10, total deposition time = 75 min) in order to obtain different Ba coverages on the substrate surface. After each deposition step, AES (30−160 eV and 30−1500 eV regions) and XPS measurements (100−60 eV region/Ba 4d, Al 2p, and Ni 3p signals, 805−775 eV region/Ba 3d signal and 542−522 eV region/O1s signal) were carried out. The C1s region (305−275 eV) in XPS was also monitored for selected deposition steps. Following the stepwise Ba deposition at 300 K, the sample was subsequently annealed at various temperatures (300 K< T < 1200 K) in UHV, for 15 min in each annealing step. After each annealing step, the sample is cooled to 300 K and the AES and XPS measurements were carried out for the energy regions described above.

3.2. AES Analysis. Figures 1 and 2 illustrate representative AES results for some of the selected steps during the Ba deposition in UHV at 300 K on the clean θ-Al_2O_3/NiAl(100) substrate and high-temperature annealing experiments. Spectrum (a) in Figure 1 corresponds to a clean NiAl(100) bimetallic alloy surface obtained after multiple sputtering−annealing cycles. The prominent AES features of the clean NiAl(100) surface are the Al_{KLL} feature at 1398 eV, the Ni_{LMM} triplet with the most intense feature appearing at 848 eV, and an unresolved feature at ~65 eV, which is a convolution of the Ni_{MVV} feature at 61 eV and the $Al^0{}_{LVV}$ feature at 66 eV. After the growth of the θ-Al_2O_3 ultrathin film on the NiAl(100) substrate, spectrum (b) of Figure 1 is obtained. In addition to the expected attenuation of the Al and Ni features due to the alumina film growth, the O_{KLL} feature originating from the oxygen-terminated[36,40] θ-Al_2O_3 film is apparent at 509 eV. Spectrum (c) in Figure 1 was acquired after depositing Ba on the clean θ-Al_2O_3/NiAl(100) surface at 300 K in UHV for 35 min, which yielded a Ba coverage slightly higher than 1 ML (ML = monolayer). Definition of the 1 ML Ba surface coverage will be discussed later in the text. It is clearly seen in Figure 1 that the introduction of Ba onto the θ-Al_2O_3/NiAl(100) substrate leads to an attenuation in the O_{KLL}, Ni_{LMM}, and Al_{KLL} features. A characteristic Ba_{MNN} doublet appears at kinetic energy (KE) values of 586 and 598 eV. Furthermore, a complex feature, which is composed of Al-, Ni-, and Ba-related features, develops at lower KE values.

Figure 2 enables a more detailed analysis of the low KE regions of the selected AES data. Spectrum (i) in Figure 2 corresponds to a clean NiAl(100) bimetallic single-crystal substrate where Ni_{MVV} and $Al^0{}_{LVV}$ features at 61 and 66 eV are better resolved than those shown in Figure 1. After the oxidation of this surface and the growth of the clean θ-Al_2O_3/NiAl(100) ultrathin film, spectrum (ii) is obtained. Features at 39, 47, and 55 eV associated with the presence of Al^{3+} states[36] are evident in addition to other poorly resolved states at 55 eV< KE < 70 eV. Spectrum (iii) represents the surface after 5 min of Ba deposition on the clean θ-Al_2O_3/NiAl(100) substrate at 300 K in UHV. As the Ni_{MVV} feature at 61 eV further attenuates, 54 and 63 eV features are better resolved. 54 and 63 eV features are attributed to convoluted Al^{3+} and Ba states where the contribution from the Ba_{MNN} states may be relatively smaller due to the low surface coverage of Ba ($\theta_{Ba} \ll 1$ ML). After 75 min of Ba deposition (spectrum (iv)), a significant change in the line shapes and the intensities of the 52, 64, and 71 eV features are observed. The intensities of these features increase with increasing Ba coverage. Hence, they are assigned to (MNN) Auger excitations of Ba. It should be also noted that at this high Ba coverage at 300 K, the intensity ratio, $I_{64\ eV}/I_{71\ eV}$, is greater than 1. An additional broad feature is also seen in spectrum (iv) around 86 eV. In a previous report[5] about Ba deposition on a Si(100) single-crystal surface, a similar feature at 85 eV was attributed to interdiffusion of Ba and Si layers to form barium silicide ($BaSi_2$). In our case, this minor feature can be attributed to the presence of a small amount of $BaAl_2O_4$ (barium aluminate) species that is formed due to diffusion of Ba into the alumina lattice. The presence of oxygen has been reported to suppress the interdiffusion of Ba and Si components to form $BaSi_2$.[5] Thus, the presence of an oxygen-terminated surface in the θ-Al_2O_3/NiAl(100) substrate may be related to the limited amount of Ba diffusion at 300 K. Spectrum (iv) also

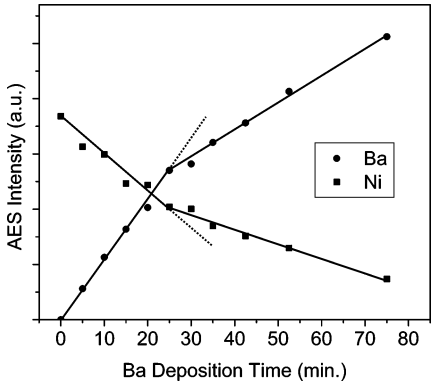

Figure 3. AES signal intensities of the Ba (MNN) feature at 598 eV and Ni(LMM) feature at 848 eV as a function of Ba deposition time. All of the Ba deposition steps (total number of steps = 10, total deposition time = 75 min) and data acquisition were carried out at 300 K in UHV.

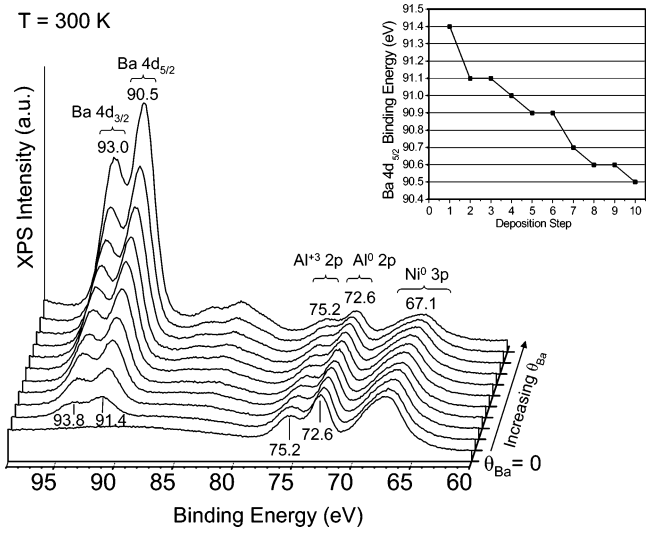

Figure 4. 100−60 eV region of the XPS data for the Ba deposition at 300 K in UHV (see text for details). Inset presents the changes in the binding energy of the Ba $4d_{5/2}$ state as a function of the deposition steps. All of the Ba deposition steps and data acquisition were performed at 300 K in UHV.

reveals that, due to the high Ba coverage and good dispersion/surface wetting (see discussion of Figure 3), the 39 and 47 eV features of the θ-Al_2O_3/NiAl(100) substrate are further suppressed. Spectra (v) and (vi) presented in Figure 2 are obtained after annealing the surface, given in spectrum (iv), at 800 and 1200 K, respectively. A clear change in the line shapes of the Ba features as well as a decrease in their AES signals are evident. Spectrum (v) and (vi) also reveal that the $I_{63\ eV}/I_{70\ eV}$ intensity ratio becomes less than 1, implying changes in the electronic structure of the Ba as well as the underlying Al^{3+} species upon annealing at 800 and 1200 K. Spectrum (vi) shows that although high-temperature annealing at 1200 K causes a significant loss in the Ba AES signal, annealing at 1200 K is not sufficient to remove all the deposited Ba from the substrate surface.

3.3. Ba Deposition at 300 K in UHV. Figure 3 illustrates absolute AES intensities of the Ba_{MNN} signal (598 eV) and the Ni_{LMM} signal (848 eV) for each of the room temperature deposition steps as a function of the total deposition time. At the early stages of the Ba deposition (t < 25 min), Ba AES signal intensity increases in a linear fashion with a constant slope until the 5th deposition step, corresponding to a total deposition time of 25 min. Meanwhile, the Ni substrate signal shows the reverse behavior during this period with a linear decrease in its intensity. After the 5th deposition step, a break point in both Ba and Ni signal intensity curves is observed. Such behavior suggests that the first Ba layer wets the θ-Al_2O_3/NiAl(100) substrate at 300 K. Thus, the Ba coverage at this break point is defined as the completion of the first Ba adlayer ($\theta_{Ba} \equiv 1$ ML). The linearly increasing behavior of the Ba signal even after the completion of the first layer (though with a different slope) implies that the layer-by-layer growth mode continues in the second adlayer as well, a result of potentially multiple factors. The wetting/dispersion of the Ba adatoms on the θ-Al_2O_3/NiAl-(100) substrate may be due to the low mobility of the Ba atoms at room temperature, preventing the surface diffusion and thus formation of 3D clusters by sintering. An oxide surface structure embodying a large number of point defect sites on its terraces may provide strong anchoring sites for the adsorbed Ba atoms and enable the formation of a well dispersed Ba adlayer. However, previous adsorption studies[32] did not support the presence of a high concentration of point defects on the alumina terraces.[42] Another reason for the layer-by-layer growth of deposited Ba on the oxygen-terminated θ-Al_2O_3/NiAl(100) substrate can be the strong attractive interaction between the oxide ions of the alumina film and the ionized Ba. This is also thermodynamically favorable as alkali earth metals have typically high free energies of oxidation ($Ba + {}^1/_2O_2 \rightarrow BaO$, $\Delta G^0_{298} = -251.1$ kcal/mol).

Figure 4 shows the 100−60 eV region of the XPS data obtained for the stepwise Ba deposition at 300 K. The spectrum belonging to the clean θ-Al_2O_3/NiAl(100) substrate before the Ba deposition is dominated by the Al^{3+} 2p feature at 75.2 eV, Al^0 2p feature at 72.6 eV, and the broad Ni^0 3p feature at 67.1 eV. After the first Ba deposition step, Ba $4d_{3/2}$ and Ba $4d_{5/2}$ XPS signals appear at 93.8 and 91.4 eV, respectively. Increasing the Ba surface coverage results in a monotonic decrease in the Ba 4d core level binding energies as illustrated by the inset of Figure 4. At the highest Ba loading of this series, Ba $4d_{5/2}$ shifts to 90.5 eV, a ΔBE of −0.9 eV with respect to its initial value obtained after the first deposition step (91.4 eV). We attribute this negative ΔBE of −0.9 eV to the growth and the partial oxidation of the barium surface component by the ionic sites of the alumina thin film substrate. It has been shown[36−40] that the θ-Al_2O_3/NiAl(100) surface is oxygen terminated where Al^{3+} cations are located about 1.4 Å below the outermost surface oxygen layer. Thus, we anticipate the extremely reactive Ba adatoms to donate charge to the Al^{3+} (cation) sites and become partially oxidized, and in this way participate in a strong ionic interaction with the O^{2-} (oxide) ions of the Al_2O_3 thin film substrate. Such a charge donation by Ba to the substrate is in agreement with the commonly observed decreasing work function of various solid surfaces upon Ba adsorption.[3,9,19,43] As the Ba coverage on the θ-Al_2O_3/NiAl(100) surface increases, Al^{3+} 2p, Al^0 2p, and Ni^0 3p features constantly attenuate without a detectable shift in their binding energy values. This is in accord with the partial oxidation of the adsorbed Ba rather than a complete oxidation and donation of a full net charge to the underlying substrate. We should emphasize that as a result of the spin−orbit splitting of the Al 2p states, the area under the XPS signal within 78−70 eV consists of at least six or more states[44] (originating from the Al^0 2p, Al^{3+} 2p, and $Al^{+(3-x)}$ 2p levels), which are poorly resolved due to our instrumental energy resolution. Thus, it is difficult to determine the exact BE positions of different Al 2p states. A synchrotron-radiation photoemission study might be able to monitor these small binding energy changes in Al 2p levels originating from the

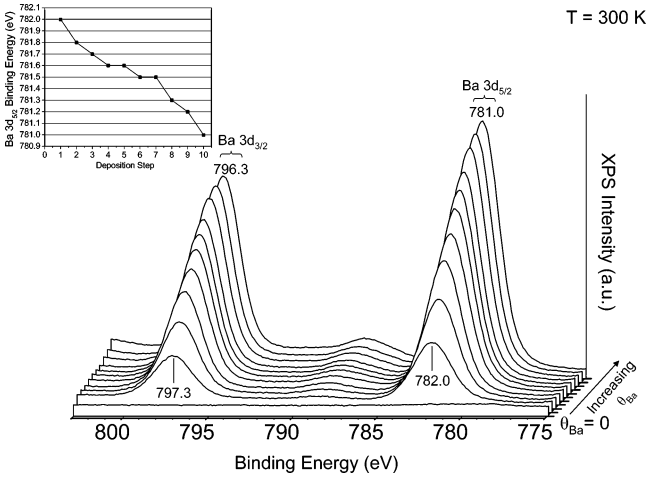

Figure 5. Evolution of the Ba 3d signals in XPS for the Ba deposition at 300 K in UHV (see text for details). Inset presents the changes in the binding energy of the Ba $3d_{5/2}$ state as a function of the deposition steps. All of the Ba deposition steps and data acquisition were performed at 300 K in UHV.

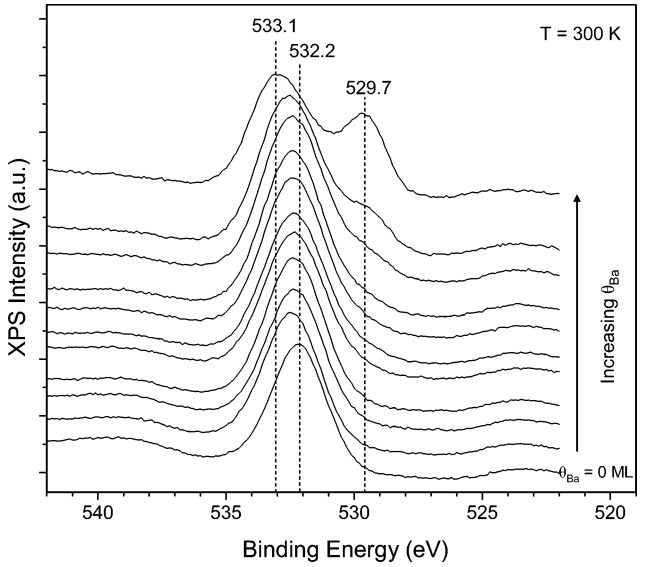

Figure 6. Evolution of the O 1s signal in XPS for the Ba deposition at 300 K in UHV (see text for details). All of the Ba deposition steps and data acquisition were performed at 300 K in UHV.

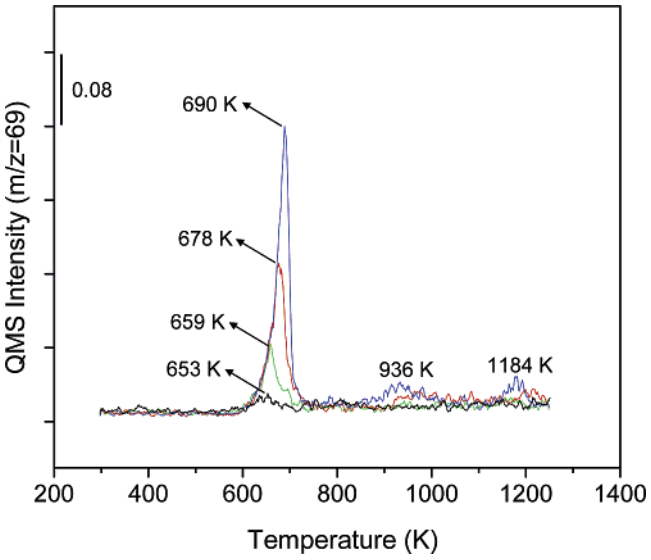

Figure 7. TPD spectra for various coverages of Ba ($\theta_{Ba} \sim 2-10$ ML) on θ-Al_2O_3/NiAl(100) surface. All of the Ba deposition steps were performed at 300 K.

partial oxidation of the deposited Ba adlayer at 300 K. Another important aspect of Figure 4 that is worth emphasizing is the increase in the baseline intensity or the secondary losses in the XPS signal with increasing Ba loading. A similar observation was previously reported during Ba deposition on an Al(111) surface[14,16] and attributed to the presence of metallic Ba states. This is in agreement with the argument that Ba atoms deposited on the θ-Al_2O_3/NiAl(100) surface are partially oxidized at 300 K and a fully oxidized BaO surface network (with continuous −Ba−O−Ba−O− linkages made of Ba^{2+} and O^{2-} ions) is not reached.

BE trends for the Ba 3d levels were also monitored during stepwise Ba deposition at 300 K. Figure 5 presents the corresponding XPS results. After the first deposition step, Ba $3d_{3/2}$ and Ba $3d_{5/2}$ peaks appear at 796.3 and 782.0 eV, respectively. With increasing Ba surface coverage, BE progressively shifts to lower values. The BE difference between the first and the last Ba deposition steps is −1 eV. It is readily seen that the BE trends observed for the Ba 3d levels are very similar to that of Ba 4d levels.

Figure 6 illustrates the O 1s region of the XPS data obtained during the stepwise Ba deposition at 300 K. The data for the clean θ-Al_2O_3/NiAl(100) substrate is given in the bottommost spectrum where a dominant feature at 532.2 eV is visible. As the Ba coverage is increased, this feature broadens noticeably and shifts to higher BE values (533.0 eV). It can be readily seen in Figure 6 that the most significant change in the O 1s region of the XPS data during the Ba deposition is the evolution of a new feature at 529.7 eV, a BE value that is 2.5 eV lower than that of the clean θ-Al_2O_3/NiAl(100) substrate. These changes in the O 1s XPS signal indicate that oxide ions of the θ-Al_2O_3/NiAl(100) surface strongly interact with the deposited Ba atoms, which results in the creation of new O 1s states. The formation of these additional O 1s states is also consistent with the partial oxidation of Ba suggested by the results given in Figures 2−5. The broadening of the O 1s signal of the θ-Al_2O_3/NiAl(100) substrate toward higher BE values (∼533.0 eV) can be attributed to the relatively less significant chemical state changes of the oxygen sites on the alumina surface that are not directly interacting or not residing in the near vicinity of the deposited Ba atoms.

3.4. Ba Desorption from the θ-Al_2O_3/NiAl(100) Surface via TPD. Figure 7 presents TPD spectra obtained for various coverages of Ba deposited on θ-Al_2O_3/NiAl(100) substrate at 300 K in UHV. It should be noted that Ba loadings used in the TPD experiments were larger (∼2−10 ML) than those used in the experiments discussed above (Figures 1−6, $\theta_{Ba} < 2$ ML). During the TPD experiments, desorbed Ba species are both singly and doubly ionized by the QMS filament; hence a 138 amu signal associated with the singly ionized Ba^+ ions as well as a 69 amu signal originating from the doubly ionized Ba^{2+} ions were monitored. Since the 69 amu signal intensities were typically higher than that of 138 amu signal, the 69 amu signal is plotted in Figure 7 (observed trends were identical for both signals). The prominent Ba desorption feature in the TPD data can be seen within 653−690 K with a zero-order desorption behavior. Thus, the desorption maxima observed within this temperature range (i.e., 650−700 K) shift to higher temperatures with increasing Ba coverage. Figure 7 reveals that, after the desorption of this low-temperature feature, additional desorption peaks are observed at higher temperatures (936 and 1184 K). Based on the discussion given in sections 3.1−3.3, as well as

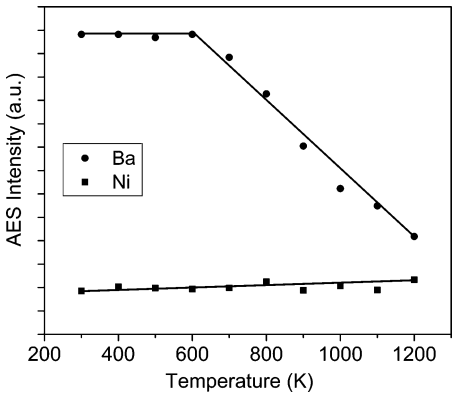

Figure 8. AES signal intensities of the Ba (MNN) feature at 598 eV and Ni(LMM) feature at 848 eV as a function of annealing temperatures (see text for details).

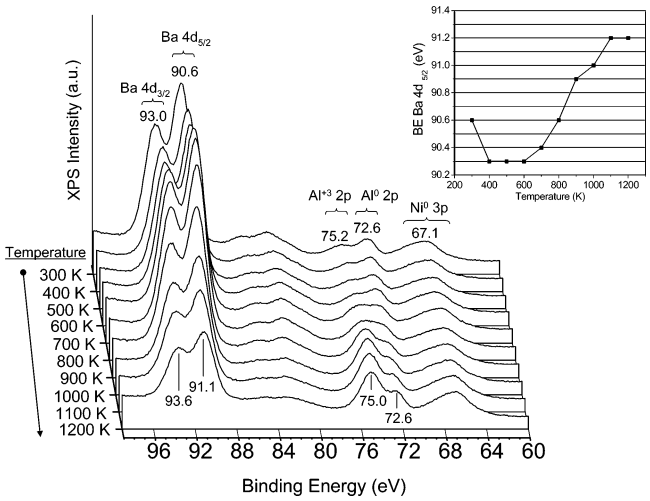

Figure 9. 100−60 eV region of the XPS data during the annealing experiments (see text for details). Inset presents the changes in the binding energy of the Ba $4d_{5/2}$ state as a function of annealing temperatures.

the further experimental evidence that will be provided in later sections, we attribute the low-temperature desorption feature at 650−700 K to metallic Ba desorption from the θ-Al_2O_3/NiAl-(100) substrate. At high Ba loadings, the first few Ba layers are partially or possibly fully oxidized within 300−700 K. These first few layers of Ba, which are strongly interacting with the surface oxide ions, are covered with weakly bound metallic Ba multilayers which desorb within 650−700 K. This explanation is in good agreement with previous TPD results for the Ba/Si-(100) system where the desorption of metallic Ba multilayers was reported at 650 K.[43,45] In Figure 7, after the desorption of the metallic Ba species, a more strongly bound Ba species starts to desorb at 936 K, which we attribute to the decomposition and desorption of oxidized Ba that is formed at elevated temperatures on the oxygen-terminated θ-Al_2O_3/NiAl(100) surface. The presence of an additional Ba TPD signal at 1184 K indicates that Ba desorption is not yet completed at 936 K and additional, even more strongly bound Ba species can exist on the θ-Al_2O_3/NiAl(100) substrate at temperatures as high as 1200 K. This observation closely resembles similar findings on the Ba/Si(100) system where a 1200 K desorption feature was assigned to the presence of Ba silicide formation at elevated temperatures.[45] However, the intensity of the 1200 K TPD signal reported in the mentioned work was significantly higher, almost twice the intensity of the 700 K feature. Therefore, we believe that this high-temperature Ba desorption signal at 1184 K can be associated with Ba diffusion into the Al_2O_3 lattice, resulting in the formation of $BaAl_2O_4$, or even diffusion into the NiAl-(100) bimetallic substrate (through a reaction that is similar to the reverse of the one given in the Experimental Section as reaction 1). Diffusion into the NiAl(100) substrate is also verified in additional experiments (not shown here) where all of the surface Ba phase and Al_2O_3 thin film were removed by sputtering and annealing cycles. After the loss of all of the Ba and O features in AES, the surface was annealed at 1200−1300 K, after which, the segregation of Ba to the surface of the NiAl(100) crystal was observed in AES by the reappearance of the Ba signal.

3.5. Thermal Behavior of the 300 K-Deposited Ba Film in UHV. Figure 8 presents absolute AES intensities of the Ba_{MNN} signal at 598 eV and the Ni_{LMM} signal at 848 eV for a sample prepared by depositing Ba on a clean θ-Al_2O_3/NiAl-(100) substrate for 75 min ($\theta_{Ba} \sim 2$ ML) at 300 K in UHV and subsequent step-by-step annealing at higher temperatures in UHV (annealing time = 15 min/step). It is apparent in Figure 8 that the Ba AES signal stays constant until 600 K and starts to decrease gradually at higher temperatures. However, no abrupt fall of the Ba AES intensity is observed within the 600−800 K range (i.e., at the temperatures where metallic multilayer Ba desorption occurs in TPD). This is because, in contrast to the TPD experiments where a high Ba loading (2 ML $< \theta_{Ba} <$ 10 ML) is used, AES data presented in Figure 8 correspond to Ba loadings less than 2 ML. Therefore, thick metallic Ba multilayers that can desorb rapidly within 650−700 K do not exist and the Ba signal in AES attenuates gradually with increasing temperature as a result of further oxidation and strong interaction of the thin Ba layer with the alumina surface at higher temperatures, as will be discussed below.

The 100−60 eV region of the XPS spectra obtained after each of the annealing steps is given in Figure 9. Binding energy values of the Ba $4d_{5/2}$ signal as a function of the annealing temperature is also plotted in the inset of Figure 9. In line with the observations given above, the Ba 4d signal intensity does not change significantly until 700 K, after which a clear monotonic decrease in the Ba 4d signal is evident. This can be readily explained by Ba desorption from the sample surface and a decrease in the Ba surface coverage. Ba desorption is also accompanied by an expected increase in the Ni 3p substrate signal intensity. Analysis of the Ba $4d_{5/2}$ BE values as a function of annealing temperature reveals the complex nature of the transformations occurring in the electronic structure of the Ba species at $T >$ 300 K (inset of Figure 9). The Ba $4d_{5/2}$ feature has a BE of 90.6 eV at 300 K. Annealing the surface at 400 K results in a binding energy shift of −0.3 eV, while no further BE shift is observed at 500 and 600 K. As the results of our AES (Figure 8), TPD (Figure 7), and XPS (Figure 9) experiments suggest, the surface coverage of Ba is not significantly altered within this low-temperature region. We assign this BE shift to further oxidation and ordering of the Ba phase on the θ-Al_2O_3/NiAl(100) substrate with thermal activation. This assignment is also supported by the AES results presented in Figure 1, suggesting a noticeable change in the electronic structure of the Ba surface species at 800 K with respect to that at 300 K. As the surface temperature reaches 700 K, the influence of the decreasing Ba coverage on the Ba $4d_{5/2}$ BE starts to be observed. Especially after annealing at 800 K, a very clear increase in the Ba $4d_{5/2}$ BE can be noticed. This BE trend continues and becomes more visible at even higher annealing temperatures where the $4d_{5/2}$ BE shifts eventually to 91.2 eV at 1200 K, which is +0.8 eV higher than the $4d_{5/2}$ BE

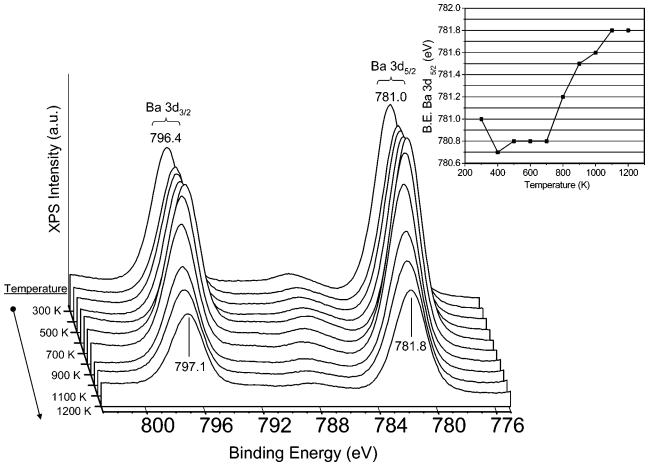

Figure 10. Evolution of the Ba 3d signals in XPS during the annealing experiments (see text for details). Inset presents the changes in the binding energy of the Ba $3d_{5/2}$ state as a function of the annealing temperatures.

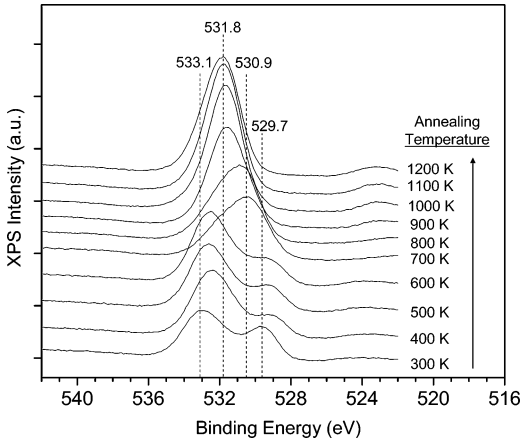

Figure 11. Evolution of the O 1s signal in XPS during the annealing experiments (see text for details).

at 300 K. This increase in BE at $T > 800$ K can be considered as a result of a decrease in Ba coverage (due to loss of Ba from the surface via desorption) and/or a change in the chemical state of the Ba species (due to a transformation from a more oxidized state to a more metallic state by loss of oxygen atoms to alumina structure or oxygen desorption to vacuum). At these high temperatures ($T > 800$ K), diffusion of Ba into the Al_2O_3 lattice to form $BaAl_2O_4$-like species cannot be excluded either.

The Al 2p region in the XPS spectra of Figure 9 also reveals important information regarding the changes that are occurring in the structure of the Ba-deposited θ-Al_2O_3/NiAl(100) substrate during the annealing steps. At 300 K, two typical features at 75.2 and 72.6 eV associated with Al^{3+} 2p and Al^0 2p states, respectively, are visible. As the Ba deposited θ-Al_2O_3/NiAl-(100) substrate is annealed at $T > 300$ K, a progressive increase in the intensity of the Al^{3+} 2p feature is noticed, in addition to a detectable BE shift to lower energy values. After the 1200 K annealing step, the Al^{3+} 2p feature is located at 75.0 eV. These observations can be attributed to a promotional effect of Ba on Al oxidation where the thickness of the alumina film increases as a result of Ba promoted reaction of the substrate Al atoms with the oxygen containing background gases such as H_2O. A simultaneous BE shift of the Al^{3+} 2p level by -0.2 eV during the growth of the intensity of the Al^{3+} 2p XPS signal also supports this argument. Ba-induced surface reconstructions at elevated temperatures and formation of $BaAl_2O_4$ as a consequence of Ba diffusion into the alumina lattice can also be responsible for the changes in the photoelectron cross sections/XPS intensities and the binding energies of the Al^{3+} 2p states.

Similar trends in the Ba 3d core levels can be seen in Figure 10 where Ba $3d_{3/2}$ and Ba $3d_{5/2}$ states are monitored during the annealing experiments. BE trends and the changes in the intensities of the Ba 3d levels are very similar to the trends seen in Figure 9. At 300 K, the Ba $3d_{5/2}$ state is located at 781.0 eV, i.e., it moves to 780.7 eV (a -0.3 eV shift) after the first annealing step at 400 K. Ba $3d_{5/2}$ BE value stabilizes at 780.8 eV within 500−700 K and starts to increase at $T \geq 800$ K, concurrent with a decrease in its intensity which can be explained using similar arguments discussed above.

The O 1s XPS signal also reveals valuable information regarding the discussion given above. Figure 11 illustrates the 540−522 eV region of the XPS spectra corresponding to the O 1s states. The bottommost spectrum of the series is obtained after Ba deposition on the clean θ-Al_2O_3/NiAl(100) substrate at 300 K (this spectrum is the same as the highest Ba loading spectrum in Figure 6). This spectrum consists of two major features at 533.1 and 529.7 eV. As discussed above, the former feature (533.1 eV) is primarily due to the O 1s states of the alumina film, which are somewhat altered with respect to the clean θ-Al_2O_3/NiAl(100) surface as a result of its interaction with Ba and related charge-transfer phenomena. The latter feature (529.7 eV) is associated with the O 1s states that are strongly interacting with the deposited Ba. Within 400−600 K, the former O 1s state shifts to 532.4−532.6 eV with intensities that remain practically constant. Similarly, the latter O 1s state shifts to 529.2 eV ($\Delta BE = -0.5$ eV). Furthermore, within this temperature interval, it is apparent that these two O 1s states become more convoluted, indicating the growth of at least one more O 1s state with a binding energy between those states. After 700 K annealing, which is just above the desorption temperature of the metallic Ba multilayers, a very significant change in the line shape of the O 1s signal is visible, which results in a broad and highly convoluted signal with a maximum at 530.9 eV. It should be noted that the AES results given in Figure 8 suggest that at this temperature the Ba coverage is still not too different from that seen at 300 K. Therefore, we attribute this significant change in the line shape in the O 1s XPS signal at 700 K to the further oxidation and ordering of the Ba species on the θ-Al_2O_3/NiAl(100) surface. This behavior also continues to a certain extent at 800 K where O 1s signal maximum shifts to 530.8 eV. However, starting from this temperature the influence of the decreasing Ba coverage as a result of decomposition of the oxidized Ba species and subsequent evaporation of metallic Ba starts to be visible. As the surface is annealed at temperatures higher than 800 K, a progressive shift of the O 1s signal to higher BE values can be observed and it settles at 531.8 eV after the 1200 K annealing step. Within 800−1200 K, a monotonic increase in the intensity of the O 1s signal is also realized, which can be attributed to the decreasing Ba coverage leading to the unveiling of the O 1s signal associated with the alumina substrate.

4. Summary and Conclusions

In this work we investigated Ba deposition on a θ-Al_2O_3/NiAl(100) substrate under ultrahigh vacuum conditions and studied the evolution of the surface species at various temperatures using different surface analysis techniques. Our results can be summarized as follows.

(a) Ba deposition on the oxygen-terminated θ-Al_2O_3/NiAl-(100) substrate at 300 K in UHV leads to layer-by-layer growth

of Ba for the first two layers, suggesting a strong interaction between the oxide ions of the alumina thin film and the deposited Ba.

(b) For $\theta_{Ba} < 2$ ML, Ba deposits are partially oxidized by the alumina substrate at 300 K. However, higher Ba coverages (2 ML$< \theta_{Ba} <$ 10 ML) result in the formation of additional metallic Ba layers which desorb from the θ-Al_2O_3/NiAl(100) surface with zero-order desorption kinetics within 650−700 K.

(c) For $\theta_{Ba} < 2$ ML, annealing the Ba deposited θ-Al_2O_3/NiAl(100) surface up to 700−800 K results in further oxidation of the Ba species. At temperatures higher than 800 K, decomposition of the oxidized Ba structure is observed, which leads to the formation of metallic-like Ba species and eventually loss of Ba from the substrate surface via desorption.

(d) After high-temperature annealing experiments, indications of Ba diffusion into the alumina lattice, probably leading to the formation of $BaAl_2O_4$ (barium aluminate) or incorporation of Ba into the NiAl(100) structure as well as Ba-promoted oxidation of the NiAl(100) substrate and thickening and/or reconstruction of the alumina film structure, were observed.

Acknowledgment. We gratefully acknowledge the U.S. Department of Energy (DOE), Office of Basic Energy Sciences, Division of Chemical Sciences for the support of this work. The research described in this paper was performed in the Environmental Molecular Sciences Laboratory (EMSL), a national scientific user facility sponsored by the DOE Office of Biological and Environmental Research and located at Pacific Northwest National Laboratory (PNNL). PNNL is operated for the U.S. DOE by Battelle Memorial Institute under contract number DE-AC05-76RL01830. The authors acknowledge with pleasure Drs. Zdenek Dohnálek and Mark Engelhard for helpful discussions.

References and Notes

(1) Newmann, N.; Lyons, W. G. *J. Supercond.* **1993**, *6*, 119.
(2) Radousky, H. B. *J. Mater. Res.* **1992**, *7*, 1917.
(3) Weitering, H. H. *Surf. Sci.* **1996**, *355*, L271.
(4) Cho, W. S.; Kim, J. Y.; Kim, S. S.; Choi, D. S.; Jeong, K.; Lyo, I. W.; Whang, C. N.; Chae, K. H. *Surf. Sci.* **2001**, *476*, L259.
(5) Fan, W. C.; Ignatiev, A. *Phys. Rev. B* **1991**, *44*, 3110.
(6) Hu, X.; Yu, Z.; Curless, J. A.; Droopad, R.; Eisenbeiser, K.; Edwards, J. L., Jr.; Ooms, W. J.; Sarid, D. *Appl. Surf. Sci.* **2001**, *181*, 103.
(7) Lee, G.; Hong, S.; Kim, H.; Koo, J. Y. *Phys. Rev. B* **2003**, *68*, 115314.
(8) Okuda, T.; An, K. S.; Harasawa, A.; Kinoshita, T. *Phys. Rev. B* **2005**, *71*, 085317.
(9) Cheng, C. P.; Hong, I. H.; Pi, T. W. *Phys. Rev. B* **1998**, *58*, 4066.
(10) Mesarwi, A.; Ignatiev, A. *J. Vac. Sci. Technol. A* **1991**, *9*, 2264.
(11) Lampert, W. V.; Rachocki, K. D.; Lamartine, B. C.; Haas, T. W. *J. Electron Spectrosc. Relat. Phenom.* **1982**, *26*, 133.
(12) Van Doveren, H.; Verhoeven, J. A. Th. *J. Electron Spectrosc. Relat. Phenom.* **1980**, *21*, 265.
(13) Wertheim, G. K. *J. Electron Spectrosc. Relat. Phenom.* **1980**, *34*, 309.
(14) Jacobi, K.; Astaldi, C.; Frick, B.; Geng, P. *Phys. Rev. B* **1987**, *36*, 3079.
(15) Barr, T. L. *J. Vac. Sci. Technol. A* **1991**, *9*, 1793.
(16) Hill, D. M.; Meyer, H. M., III; Weaver, J. H. *Surf. Sci.* **1990**, *225*, 63.
(17) Vasquez, R. P. *J. Electron Spectrosc. Relat. Phenom.* **1991**, *56*, 217.
(18) Pacchioni, G.; Sousa, C.; Illas, F.; Parmigiani, F.; Bagus, P. S. *Phys. Rev. B* **1993**, *48*, 11573.
(19) Pi, T. W.; Hong, I. H.; Cheng, C. P. *Phys. Rev. B* **1998**, *58*, 4149.
(20) Zhang, C.; Wang, L.; Cui, L.; Zhu, Y. *J. Cryst. Growth* **2003**, *255*, 317.
(21) Gaarenstroom, S. W.; Winograd, N. *J. Chem. Phys.* **1977**, *67*, 3500.
(22) Hrbek, J.; Yang, Y. W.; Rodriguez, J. A. *Surf. Sci.* **1993**, *296*, 164.
(23) Branda, M. M.; Di Valentin, C.; Pacchioni, G. Y. *J. Phys. Chem. B* **2004**, *108*, 4752.
(24) Fournier, V.; Marcus, P.; Olefjord, I. *Surf. Interface Anal.* **2002**, *34*, 494.
(25) Epling, W. S.; Campbell, L. E.; Yezerets, A.; Currier, N. W.; Parks, J. E., II *Catal. Rev.* **2004**, *46*, 2, 163 and references therein.
(26) Nova, I.; Castoldi, L.; Prinetto, F.; Dal Santo, V.; Lietti, L.; Tronconi, E.; Forzatti, P.; Ghiotti, G.; Psaro, R.; Recchia, S. *Top. Catal.* **2004**, *30−1*, 181.
(27) Olsson, L.; Blint, R. J.; Fridell, E. *Ind. Eng. Chem. Res.* **2005**, *44*, 3021.
(28) Matsumoto, S. *Cattech.* **2000**, *4*, 102.
(29) Heck, R. M.; Farrauto, R. J. *Catalytic Air Pollution Control: Commercial Technology;* International Thomson Publishing: New York, 1995.
(30) Ozensoy, E.; Goodman, D. W. *Phys. Chem. Chem. Phys.* **2004**, *6*, 3765.
(31) Stone, P.; Ishii, M.; Bowker, M. *Surf. Sci.* **2003**, *537*, 179.
(32) Ozensoy, E.; Szanyi, J.; Peden, C. H. F. *J. Phys. Chem. B* **2005**, *109*, 3431.
(33) Ozensoy, E.; Peden, C. H. F.; Szanyi, J.; *J. Phys. Chem. B* **2005**, *109*, 15977.
(34) Ozensoy, E.; Peden, C. H. F.; Szanyi, J.; *J. Phys. Chem. B*, submitted.
(35) Ozensoy, E.; Peden, C. H. F.; Szanyi, J.; *J. Phys. Chem. B* **2006**, *110*, 17009.
(36) Gassmann, P.; Franchy, R.; Ibach, H. *Surf. Sci.* **1994**, *319*, 95.
(37) Gassmann, P.; Franchy, R.; Ibach, H. *J. Elec. Spec. Relat. Phenom.* **1993**, *64/65*, 315.
(38) Fremy, N.; Maurice, V.; Marcus, P. *J. Am. Ceram. Soc.* **2003**, *86*, 669.
(39) Fremy, N.; Maurice, V.; Marcus, P. *Surf. Interface Anal.* **2002**, *34*, 519.
(40) Maurice, V.; Fremy, N.; Marcus. P. *Surf. Sci.* **2005**, *581*, 88.
(41) Most of the water soluble Ba compounds are toxic. For example $BaCO_3$ is used as rat poison. Thus, materials including Ba should be handled with care.
(42) It is known in the literature that θ-Al_2O_3 ultrathin films grown on NiAl(100) substrates exhibit orthogonal domains where there exist extended line defects, steps, and edges (for example, see refs 38−40). Thus, as an alternative explanation for Figure 3 (with an assumption that the Ba adatoms have enough surface mobility), the break point can be attributed to an initial decoration of the step edges followed by the saturation of these extended defects and the beginning of the population of the energetically less favorable terrace sites. However, considering the Ba XPS signal intensities and the corresponding attenuation of the Al^{3+} XPS signal at $t = 25$ min in Figure 4, we believe that the total Ba coverage at $t = 25$ min is well above the relatively smaller number of available extended defect sites.
(43) Vlachos, D. S.; Papageorgopoulos, C. A. *J. Phys.: Condens. Matter* **1996**, *8*, 8799.
(44) Jaeger, R. M.; Kuhlenbeck, H.; Freund, H. J.; Wuttig, M.; Hoffmann, W.; Franchy, R.; Ibach, H. *Surf. Sci.* **1991**, *259*, 235.
(45) Vlachos, D.; Kamaratos, M.; Papageorgopoulos, C. *Solid State Commun.* **1994**, *90*, 175.
(46) Altieri, S.; Tjeng, L. H.; Sawatzky, G. A. *Thin Solid Films* **2001**, *400*, 9 and references therein.
(47) Bagus, P. S.; Pacchioni, G.; Sousa, C.; Minerva, T.; Parmigiani, F. *Chem. Phys. Lett.* **1992**, *196*, 641.
(48) Sousa, C.; Minerva, T.; Pacchioni, G.; Bagus, P. S.; Parmigiani, F. *J. Electron Spectrosc. Relat. Phenom.* **1993**, *63*, 189.